APEM journal
Advances in Production Engineering & Management
Volume 16 | Number 4 | December 2021 | pp 457–472
https://doi.org/10.14743/apem2021.4.413
ISSN 1854-6250
Journal home: apem-journal.org
Original scientific paper

Molecular-dynamics study of multi-pulsed ultrafast laser interaction with copper

Yin, C.P.[a], **Zhang, S.T.**[a], **Dong, Y.W.**[a,*], **Ye, Q.W.**[a], **Li, Q.**[b]

[a]School of Aerospace Engineering, Xiamen University, Xiamen, P.R. China
[b]ENN Energy Power Technology (Shanghai) Co., Ltd, Shanghai, P.R. China

ABSTRACT

Ultrafast laser has an undeniable advantage in laser processing due to its extremely small pulse width and high peak energy. While the interaction of ultrafast laser and solid materials is an extremely non-equilibrium process in which the material undergoes phase transformation and even ablation in an extremely short time range. This is the coupling of the thermos elastic effect caused by the pressure wave and the superheated melting of the material lattice. To further explore the mechanism of the action of ultrafast laser and metal materials, the two-temperature model coupling with molecular dynamics method was used to simulate the interaction of the copper and laser energy. Firstly, the interaction of single-pulsed laser and copper film was reproduced, and the calculated two-temperature curve and the visualized atomic snapshots were used to investigate the influence of laser parameters on the ablation result. Then, by changing the size of the atomic system, the curve of ablation depth as a function of laser fluence was obtained. In this paper, the interaction of multi-pulsed laser and copper was calculated. Two-temperature curve and temperature contour of copper film after the irradiation of double-pulsed and multi-pulsed laser were obtained. And the factors which can make a difference to the incubation effect were analyzed. By calculating the ablation depth under the action of multi-pulsed laser, the influence of the incubation effect on ablation results was further explored. Finally, a more accurate numerical model of laser machining metal is established and verified by an ultra-short laser processing experiment, which provides a new calculation method and theoretical basis for ultra-fast laser machining of air film holes in aviation turbine blades, and has certain practical guiding significance for laser machining.

ARTICLE INFO

Keywords:
Ultrafast laser,
Multi-pulsed laser;
Ablation;
Copper;
Modelling and simulation;
Two-temperature model;
Molecular dynamics;
Laser machining

**Corresponding author:*
yiweidong@xmu.edu.cn
(Dong, Y.W.)

Article history:
Received 22 September 2021
Revised 22 November 2021
Accepted 3 December 2021

1. Introduction

Ultrafast laser ablation, which uses ultrafast laser to remove the surface of solid materials, with processing accuracy ranging from micron to nanometer scale, which allows material processing with extremely high precision due to the relatively small heat affected zone from each pulse [1]. This feature makes the ultrafast laser have the advantage of 'cold processing' which means the thermal influence on the surrounding material is extremely small. The surrounding material is still in a 'cold state' while the electron temperature in the processed region reaches an extremely high level from the solid state to the plasma state, which ensures the processing edge is neat [2]. In addition, due to the distribution characteristics of the Gaussian laser, the size of the ultrafast laser processing can be smaller than the spot size of the laser to achieve microfabrication. In the process of ultrafast laser processing, the absorption of laser light by the material is multiphoton absorption [3], which is more dependent on the atomic properties of the material. This feature

makes the range of materials for femtosecond laser processing no longer limited. Ultrafast lasers have the above-mentioned significant advantages in the microfabrication process of materials, while the further improvement in processing technology and precision is limited by the complexity of its mechanism of action. In the process of ultrafast laser action, electronic excitation, internal heat transfer of materials and melting of materials are involved. Fig. 1 shows an overview of the physical phenomena involved in the time range considered.

The main methods used by domestic and foreign scholars of ultrafast laser ablation of solid materials can be divided into numerical simulation and experimental determination.

Numerical simulation is widely used because of its low cost, good reflection of physical processes, and ease of analysis. Annemie [4] *et al*. simulated atomic-scale material failures such as melting, vaporization and spallation by combining molecular dynamics (MD) and finite difference methods, derived the spatiotemporal evolution of density and pressure through the two-temperature model (TTM), then discussed the heat transfer of the special alloy with anisotropy, and calculated and verified the electron cooling time and ablation threshold. Ivanov [5] *et al*. presented an atomistic-to-continuum (AtC) computational model to investigate the dynamic microscopic mechanism of laser ablation of nickel and gold films. It is found that the interaction between the growth front of the melting front end of the film (liquid-crystal interface) and the uniform nucleation of the liquid phase inside the crystal is the reason that the laser fluence near the melting threshold causes the metal film to melt. At higher laser fluence, the high tensile stress generated inside the film is also a cause of cracking. Foumani [6] *et al*. used a TTM-MD method to investigate the response of copper film at different laser fluences. Based on the model, the dependence of the reflectivity of the copper film on the laser fluence and the evolution of density, electron temperature and lattice temperature with time were obtained. Porvanitsy [7] *et al*. used two different methods to simulate the laser ablation of aluminum bulks by changing the laser fluence. The first method is single-fluid two-temperature hydrodynamics (HD) completed with a two-temperature equation of state (EOS), the second approach is a combination of classical molecular dynamics and a continuum model of a free electron subsystem. After comparing the simulation results with the experiment, it is found that the HD and MD methods show good consistency in describing the phase explosion and cracking process. The TTM is a mainstream model for exploring the effects of metals and ultrafast lasers. The researchers have continuously improved and reduced the TTM [8] to apply to calculations in different materials and different media.

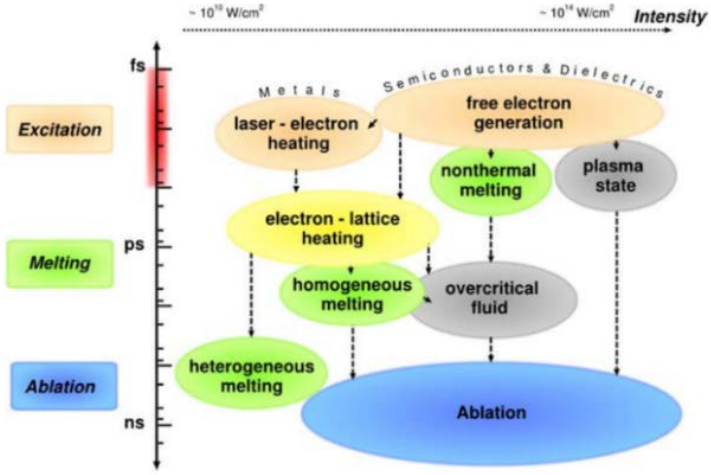

Fig. 1 Physical phenomena involved in the action of ultrafast lasers and solid materials [2]

In the field of multi-pulsed laser ablation, researchers often use experimental methods to study the changes of hole depth and hole morphology with incident laser parameters. Winter [9] *et al*. used the experimental method to ultra-fast measurement of the refractive index of copper. At the same time, the TTM and thermo-mechanical model with precise description of thermal and optical properties were used as theoretical support to explore the refractive index n and the extinction coefficient k in different time ranges. Wang [10] *et al*. used a double-pulsed femtosecond laser to

irradiate copper and aluminum films of 50 μm. It has been found that both the copper film and the aluminum film pore size decrease as the double pulse delay increases, but the diameters of the redeposited materials of the two films are different. Karim [11] *et al*. studied the interaction between short-pulsed lasers and metal surfaces with solid transparent coatings by combining experimental and atomic simulations and revealed the structural modification mechanism of the junction zone between metal and coating. Fokin [12] *et al*. used TTM-HD and TTM-MD method to clarify the reaction mechanism of metal targets on laser irradiation.

In this paper, the TTM-MD method is used to simulate the metal copper film irradiated by single-pulsed and multi-pulsed laser. We explored the factors that influence the ablation results and the ablation depth at different laser fluences under the action of a single pulsed laser. Then, the simulation of multi-pulsed laser ablation of metals reveals the existence of incubation effects and its effects on ablation depth.

2. Computational model

2.1 TTM-MD model for Cu target

When we describe the change of the metal after exposure to laser light, the energy transfer from the electron to the lattice is slow due to the large mass difference between the electron and the phonon [13]. Therefore, it is unreasonable to assume that the electron and the lattice temperature are the same when the duration of the laser pulse is no longer than the time at which the electron and the lattice reach equilibrium. The two-temperature model proposed by Anisimov [14] in 1973 is a good description of the time evolution of electron and lattice temperatures of metals under ultrafast laser irradiation. In recent years, TTM has become an effective model for studying the evolution of electron and lattice temperature with time under the action of ultrafast lasers. The two one-dimensional nonlinear differential equations are as follows:

$$c_e \frac{\partial T_e}{\partial t} = \frac{\partial}{\partial x}\left(k_e \frac{\partial T_e}{\partial x}\right) - g(T_e - T_i) + S(x,t) \tag{1}$$

$$c_i \frac{\partial T_i}{\partial t} = g(T_e - T_i) \tag{2}$$

Where T_e is the temperature of the electronic system and T_i is the temperature of the lattice system. The first term on the right side of Eq. 1 is the heat conduction term, the second term is the energy coupling term, and the third term is the laser source term. When using a Gaussian beam for numerical simulation, the source term can be rewritten as [15]:

$$S(x,t) = \frac{A\alpha F}{\sqrt{\pi/4\ln(2)}\tau_L} \exp(-\alpha x) \cdot \exp[-4\ln(2)(t/\tau_L - 2)^2] \tag{3}$$

Where A is the surface transmittance α, is the material absorption coefficient, F is the laser fluence, x is the depth from the calculated position to the surface of the material, and τ_L is the pulse width. When double-pulsed or multi-pulsed laser is used, the light source term can be rewritten as [16]:

$$S(x,t) = \frac{A\alpha F}{\sqrt{\pi/4\ln(2)}\tau_L} \exp(-\alpha x) \cdot \exp[-4\ln(2)(t/\tau_L - 2)^2 - 4\ln(2)((t - dt_1)/\tau_L - 2)^2] \tag{4}$$

$$S(x,t) = \frac{A\alpha F}{\sqrt{\pi/4\ln(2)}\tau_L} \exp(-\alpha x) \cdot \exp[-4\ln(2)(t/\tau_L - 2)^2 - 4\ln(2)((t - dt_1)/\tau_L - 2)^2 - 4\ln(2)((t - dt_2)/\tau_L - 2)^2] \tag{5}$$

where dt_1 and dt_2 are the pulse interval time, respectively.

Although the two-temperature model is widely used to explore ablation mechanisms, predict ablation thresholds and many other research fields, there are still deficiencies. Especially in describing the phase transition of metal material continuum under high imbalance conditions, it often involves many assumptions and simplifications. There are many controversies about the phase transition mechanism under intense overheating, which requires TTM to be combined with other methods to perform more accurate simulations.

Therefore, we introduce molecular dynamics simulation. The significant advantage of molecular dynamics over hydrodynamic is that its priori includes nucleation kinetics and phase transitions without any assumptions about nucleation kinetics. This solves the shortcomings of the two-temperature model described before, so MD is suitable for the calculation of small scale fast unbalanced processes. The MD simulation assumes that all particles satisfy Newton's second law and are subject to the forces of other particles, this interaction satisfies the principle of superposition. The MD simulation process is to calculate the potential energy of the system under the given initial conditions, iteratively solve the motion equation to obtain the position information and spatial coordinates of the particles, and select the appropriate difference formula to calculate the potential energy. Then the spatial information of the particles will be newly calibrated by the constraint algorithm of temperature and pressure.

The classical molecular dynamics method only considers the lattice thermal conduction, but the electron conduction in the metal dominates, so it underestimates the total thermal conductivity of the metal, and cannot be directly used to simulate the interaction between metal and ultrafast lasers without two-temperature model. The TTM-MD equations we used are shown as following [17]:

$$c_e(T_e)\frac{\partial T_e}{\partial t} = \frac{\partial}{\partial x}\left(k_e(T_e)\frac{\partial T_e}{\partial x}\right) - g(T_e - T_i) + S(x,t), \quad \text{TTM} \tag{6}$$

$$m_i\ddot{r}_i = F_i + \xi m_i V_i^T, \quad \text{MD} \tag{7}$$

$$\xi = \frac{1}{n}\sum_{k=1}^{n} gV_N\left(T_e^k - T_l\right) / \sum_i m_i\left(V_i^T\right)^2 \tag{8}$$

where m_i and r_i are the mass and position of the ith atom, respectively, F_i is produced by the interaction between atoms, that is, the force generated on the ith atom. The additional item $\xi m_i V_i^T$ in the equation is brought by electron-phonon coupling. The thermal motion velocity V_i^T in this term is different from the velocity V representing the atom in the whole system, which is generally a function of temperature. The lattice temperature and energy coupling coefficient ξ are determined by each unit cell and summed. The TTM-MD method not only explains the electron energy absorption, the energy exchange process between electrons and phonons, but also provides the possibility to describe the non-equilibrium ablation process when the lattice is overheated.

2.2 Calculation parameters

In this calculation we need to choose the appropriate potential function and set the periodic boundary conditions. The potential function between molecules represents the force of interaction between molecules, and the gradient of the potential function is the force function. In this calculation we use the metal potential function EAM (embedded-atom model), the mathematical expression [15] of the model is as follows:

$$u_{EAM} = \sum_{i=1}^{N}\sum_{j=i+1}^{N} u\left(r_{ij}\right) + \sum_{i=1}^{N} E(\rho_i) \tag{9}$$

The first term on the right side of Eq. 9 is the two-body potential between the nucleus, the second item is the mosaic energy of the nucleus, which is the result of multi-body action. According to the density functional theory (DFT), the nucleus is affected by other nuclei, and is also subjected to the multi-body effect in the background of the electron cloud, which is the second term of the equation.

Due to the limitation of computing resources, periodic boundary conditions are used in this calculation. Because of the existence of periodic boundary conditions, the particles can not only move in the central cell, but after the particles move out of one side boundary at a certain speed, they will enter the central cell at the same speed from the other side, to ensure a certain number of atoms and eliminate the boundary effect. The calculation model after applying periodic boundary conditions is shown in Fig. 2.

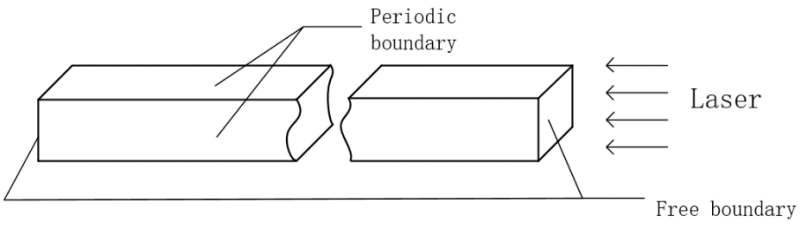

Fig. 2 Schematic diagram of boundary conditions of the model

In this paper, pure copper crystal is used for simulation of ultrafast laser ablation. When investigating the effect of pulse parameters on temperature changes and ablation results, the model size is $6a \times 6a \times 150a$, the lattice parameter of copper is $a = 0.3615$ nm, the copper crystal is a face-centered cubic structure, so the actual central cell model is 2.619 nm × 2.619 nm × 54.225 nm and the number of atoms is 21672. When calculating the ablation depth, in order to avoid the influence of thermal expansion caused by the system being too small, the model is expanded to 2.619 nm × 2.619 nm × 361.5 nm, and the number of atoms is expanded to 144072. The thermal property parameters of copper are derived from the 'Cu_ttm.mat' file in LAMMPS (LAMMPS Molecular Dynamics Simulator), in which the specific heat of the electron and the specific heat of the lattice are set to be constant, the electron-phonon coupling coefficient and the thermal conductivity of electrons and lattice are approximately linearly related to temperature.

Before the laser is incident during the simulation, the copper atoms in the system are relaxed and balanced at 300 K, and a total of 100,000 steps are performed in time step of 0.001 ps. In this way, the structural order parameters of the system are close to 1, and the atomic velocity distribution inside the system is Maxwell distribution at 300 K, which ensures the accuracy of the initial simulation system and the reliability of the calculation results.

3. Results and discussion

3.1 Interaction of single-pulsed laser with cooper film

In this section, firstly we reproduced the simulated laser ablation process of single-pulsed laser with copper film, compared the results with existing literature [16] and further changed the parameters of laser to explore the mechanisms of ablation. Ablation depths under different laser fluences are also considerable for our research.

The comparison of the following temperature contours directly reflects the correctness and reliability of our simulation calculation. We selected the same laser parameters and potential function as the existing literature [16] in the calculation process. As shown in Figs. 3 and 4, the maximum electron temperatures are 16000 K both, the thermal influential area is 5 nm away from the incident surface of the laser, and the highest temperature can reach is more than 15000 K in the two pictures. Since the electron specific heat used in this paper is a fixed value and smaller than the linear relationship of $C_e = 96.6\ T_e$ (J/m^3·K) used in the comparison literature, the time it takes for the electron to reach the highest temperature is shorter.

Comparing Figs. 3 and 4, we found that since the electron-phonon coupling factor of this paper is slightly higher than 1×10^{17} (W/m^3·K) used in the comparative literature [16], the lattice can reach its highest temperature faster. However, the thermal conductivity of the lattice is lower than the linear relationship simulated in the literature, so the highest temperature that the lattice can reach is lower than the comparative literature. In summary, this simulation is accurate and effective within the consideration of the selected parameters.

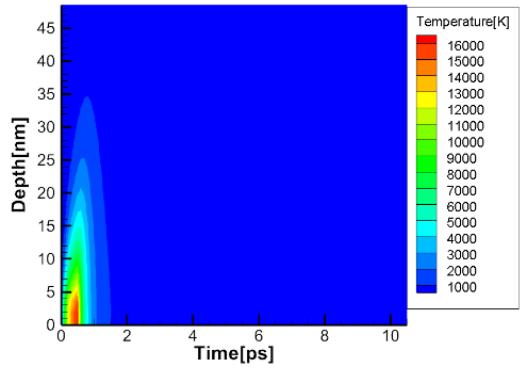

Fig. 3 Electron temperature contour with pulse width of 500 fs and laser fluence of 320 J/m²

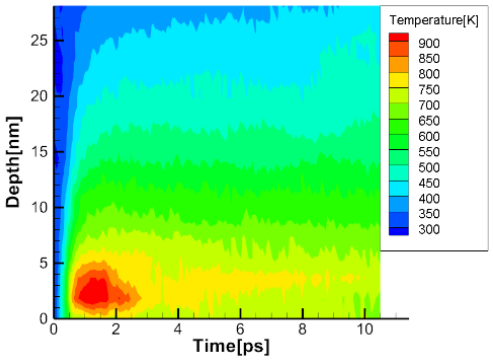

Fig. 4 lattice temperature contour with pulse width of 500 fs and laser fluence of 320 J/m²

Different influence factors for ablation results

Laser pulse width and laser fluence are two important factors affect the ablation results, to explore the mechanism of the action between laser and copper film, we changed these two parameters and make the laser source perpendicular to the $z = 0$ surface to obtain different two-temperature curves. In the first set of calculations, the fixed laser fluence is 1000 J/m², and the pulse width is selected to be 100 fs, 300 fs, and 500 fs, respectively.

The temperature shown in Figs. 5 to 8 are all refer to the average temperature. It can be seen in Fig. 5 that at 0.5 ps, the electron reached a maximum temperature of 6010 K, and then the energy obtained by electron transferred to the lattice by electro-phonon coupling, so the temperature of electron rapidly fell back. The lattice reached a peak temperature of 522 K at about 1.6 ps, after which the temperatures of the electron and the lattice tend to coincide. In Figs. 6 and 7, the electron reached peak temperature of 7642 K and 9767 K at 0.3 ps and 0.1 ps, respectively. And the process of electron-phonon coupling leading to a balance of electron and lattice temperature is highly consistent with the process shown in Fig. 5.

As can be seen from Fig. 8, the smaller the pulse width of the incident laser, the shorter the time required for the electron to reach the peak temperature, and the higher the peak temperature of the electron. This is because a small pulse width means a more concentrated pulse energy power, and the calculated electron and lattice equilibrium temperature for each calculation is constant because the laser fluence is a fixed value for the energy injected into the system.

Taking the calculation at pulse width 300 fs as an example, the electron and lattice temperature curves at the farthest end of the laser incident surface at z = 54.225 nm and the laser incident surface at z = 0 are analyzed, we obtain the two-temperature curves as shown in Figs. 9 and 10:

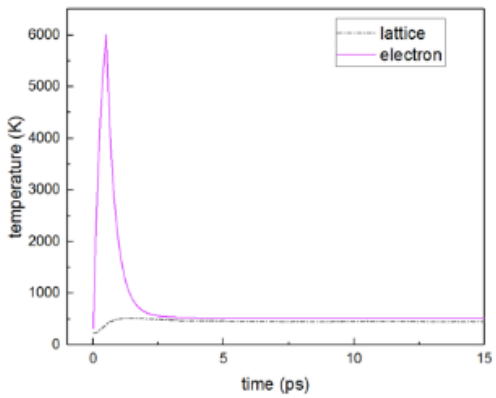

Fig. 5 Two-temperature curve with laser fluence of 1000 J/m² and pulse width of 500 fs

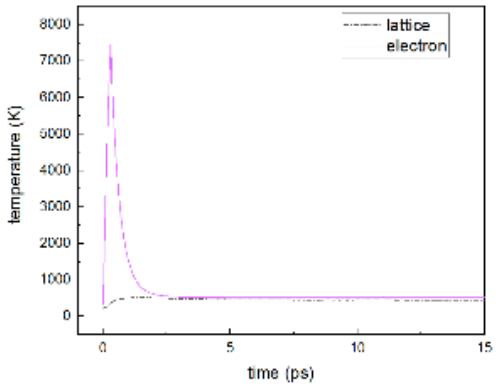

Fig. 6 Two-temperature curve with laser fluence of 1000 J/m² and pulse width of 300 fs

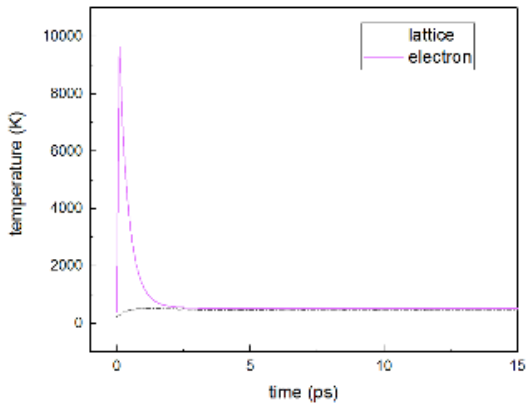

Fig. 7 Two-temperature curve with laser fluence of 1000 J/m^2 and pulse width of 100 fs

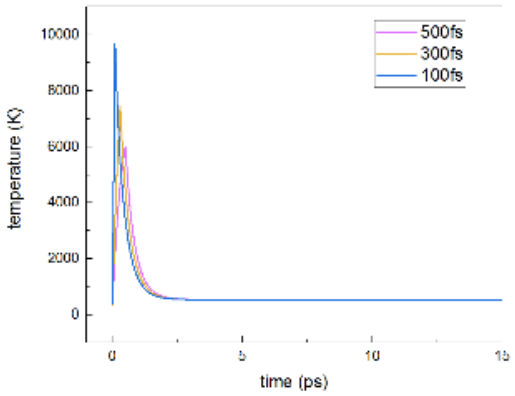

Fig. 8 Electron temperature curves with different pulse widths at laser fluence of 1000 J/m^2

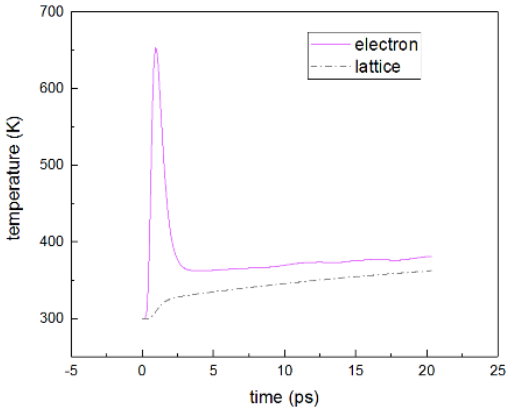

Fig. 9 Two-temperature curve at z = 54.225 nm

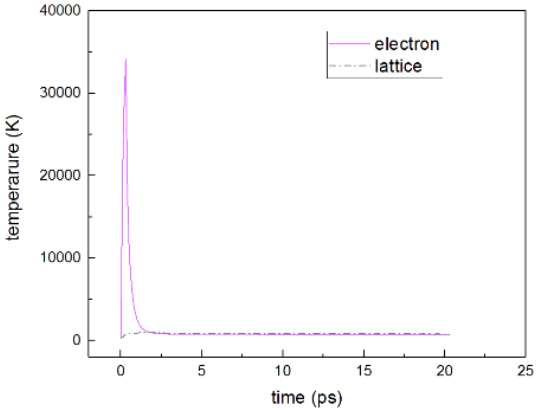

Fig. 10 Two-temperature curve at z = 0

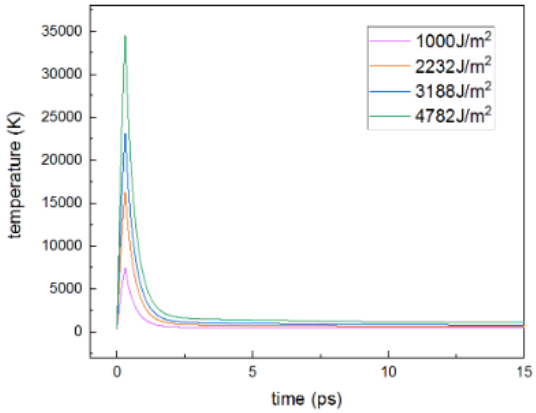

Fig. 11 Temperature change of electron

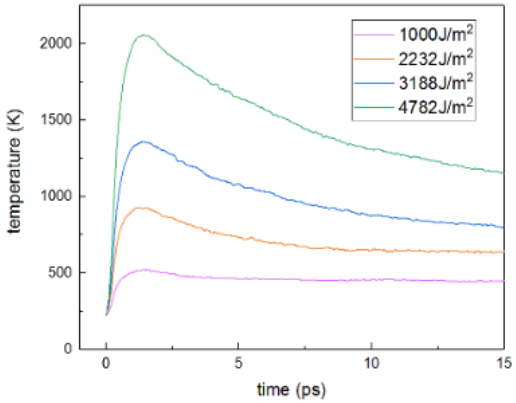

Fig. 12 Temperature change of lattice

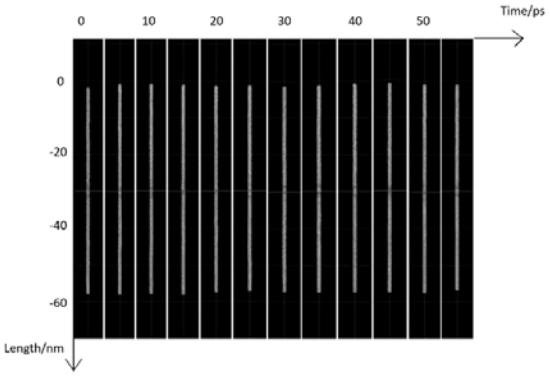

Fig. 13 Atomic snapshots at a laser fluence of 1000 J/m^2

The electron on the laser incident surface shown in Fig. 10 rapidly rose to 34147 K at 0.3 ps, and the lattice reached a maximum temperature of 1028 K at 1.4 ps. In the bottom region of the model, which is less affected by heat, the electron reached a maximum temperature of 653 K at 0.9 ps, after which the cooled electron and the lattice would keep the same rising trend of temperature due to the heat conduction from the front face. This is consistent with the change in the average temperature of the entire system.

In another set of calculations, we fixed the laser pulse width to 300 fs to obtain the two-temperature curves with different laser fluences of 1000 J/m^2, 2232 J/m^2, 3188 J/m^2 and 4782 J/m^2 as shown in the Figs. 11 to 12. It can be easily seen that an increase in laser fluence can cause an increase in electron and lattice temperature.

To clearly understand the ablation process, the trajectories of all atoms were imported in-to Visual Molecular Dynamics (VMD) for visualization. As shown in Fig. 13, when the laser fluence is small as 1000 J/m^2, no ablation occurs, and the energy is not enough to cause phase transformation of the material. However, it can be seen the film undergoes periodic elongation and shortening un-der the action of laser from the visualization results. The periodic expansion and contraction of the film under the action of internal stress waves is known as the 'film respiration' phenomenon [16]. The film was rapidly heated and expanded within 0-15 ps after being irradiated by the laser. During this time, since the heating time of the lattice is less than the time when the thermal expansion occurs, the compressive stress transmitted from the upper surface to the lower surface will be generated inside the film. After transmitting to the lower surface, a tensile stress wave of negative reflection was formed, then the tensile stress wave caused by thermal expansion and the tensile stress wave formed by negative reflection were superimposed on each other to promote expansion of the film during this period. The tensile stress wave would decrease as the film linear expansion value reached a maximum. At 15-30 ps, the tensile stress wave continued to weaken and the compressive stress wave was still forming, and the film began to shrink. After the film reached equilibrium at around 30 ps, it began to periodically expand and contract, and expanded to a maximum at 45 ps. Such a peri-odic action consumes the injected energy when the laser energy is insufficient to cause ablation.

As the laser fluence increases to 2232 J/m^2 shown in Fig 14, when the material is exposed to energy-concentrated ultrafast laser, an extremely non-equilibrium process occurs. The electrons were rapidly heated by the collision between the electrons after quickly absorbing a large amount of photon energy. At the same time, the lattice has not warmed up while its temperature was still close to room temperature. This will cause the unheated crystal lattice to be subjected to a strong force from the potential energy surface [17] (PES), which is usually affected by the effective potential of electrons acting on the ions. After the action of the force, the ions began to move and caused the material to be disordered rapidly. Usually, this ultra-fast disorder is considered to be a melting process. The front end of the material melts, some of the atoms are ablated from the surface of the material, and the material has a relatively obvious thermal expansion effect.

As the laser fluence becomes 3188 J/m^2, ablation is more severe as shown in Fig. 14, the atomic clusters began to break away from the system. Usually, the melting occurs at the disappearance of the heterogeneous nucleation barrier on the surface of the material and then propagates inside the material at a speed less than the speed of sound of hundreds of meters per second. In the case of sufficient overheating (overheating ratio greater than 1.5), it is also possible to produce a uniform nucleation melting phenomenon. The nucleation inside the material can be observed at -8 nm in Fig. 15. Further increase the laser fluence as Fig. 16 shown the more intense mechanical stress caused by thermal expansion and the melting generated inside the material cause the film to crack. Compared with the ablation at lower laser fluence in Fig. 15, the ablation depth increases and the linear expansion rate also increases significantly.

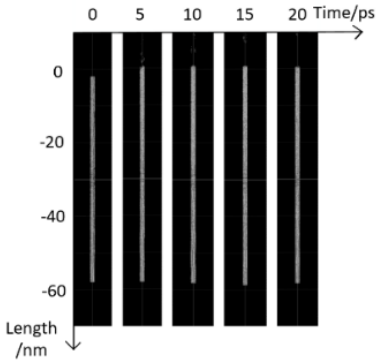

Fig. 14 Atomic snapshots at a laser fluence of 2232 J/m²

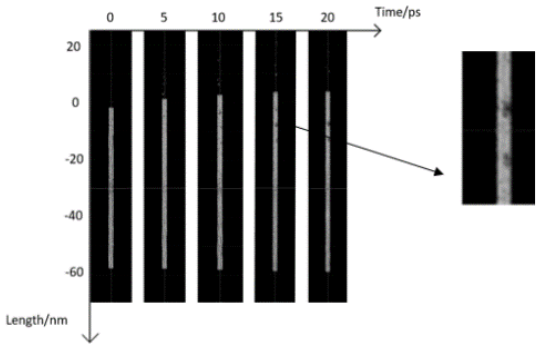

Fig. 15 Atomic snapshots at a laser fluence of 3188 J/m²

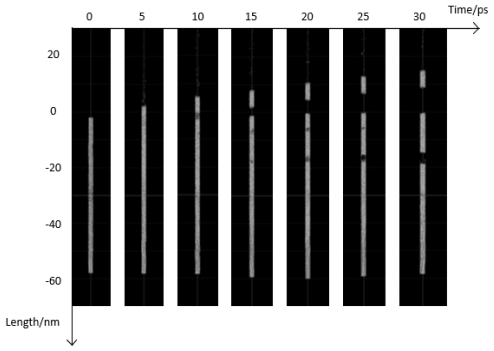

Fig. 16 Atomic snapshots at a laser fluence of 4782 J/m²

Ablation depths under different laser fluences

To understand the ablation process better, it is necessary to correlate the numerical simulation results with the actual drilling process and calculate the ablation depth. We increased the model size and the time step of the calculation to obtain more efficient simulation results. It's the way to ensure that the system is large enough to keep the atomic temperature of the bottom surface from being affected by heat at room temperature and make the simulation close to real processing conditions. We mainly explore the influence of the difference of laser fluence on the ablation depth of copper film, the pulse width for our simulation is a fixed value of 300 fs and the four parameters 3188 J/m², 4782 J/m², 6377 J/m², and 7971 J/m² are used to obtain the curve as shown as Fig. 17. The other curve in the figure is from the experimental data of the comparative literature [18]. The experimental curve obtained in the experiments of the literature [18] is shown in Fig. 18. Within the laser fluence range calculated in this paper, the ablation depth of the material exhibits an approximately linear relationship with the laser fluence. It can be seen that in the range of laser fluence simulated in this paper, the calculated value of the ablation depth is highly consistent with the experimental values in the comparative literature. Obviously, the ablation caused by single pulse is in the order of nanometers, and there is a certain gap with the actual processing needs in engineering. Therefore, it is necessary to carry out numerical simulation of multi-pulsed laser ablation of metal copper film.

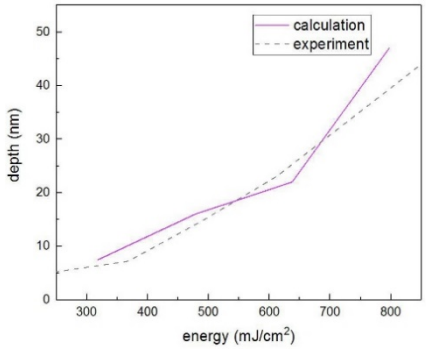

Fig. 17 Ablation depth changed by laser fluence

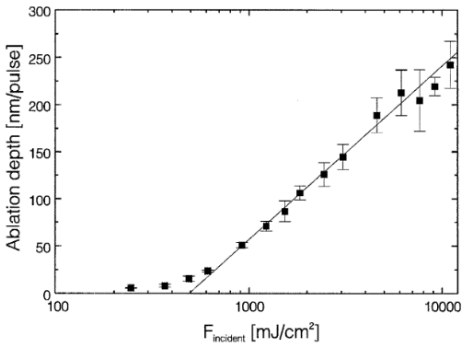

Fig. 18 Ablation depth changed by laser fluence [19]

3.2 Interaction of double-pulsed and multi-pulsed laser with copper film

In recent years, domestic and foreign scholars have done some research on the interaction of single-pulsed and double-pulsed with metal, while the field of multi-pulsed laser action on metal is less involved due to its extremely complex internal mechanism.

To explore the interaction of multi-pulsed laser and metal, we must explain the concept of ablation thresholds [19] firstly. The ablation threshold refers to the laser fluence required for the laser to irreversibly destroy the metal and remove the surface of the material during the ultrafast laser action of the metal. Usually, a certain value is obtained during the single-pulsed laser ablation of the metal, but as the number of pulses increases, the ablation threshold of the material will be inversely proportional to the number of pulses. The ablation process of the material can also be done with a small laser fluence, which is called the incubation effect [20], and its mathematical expression is:

$$F_{th}(N) = F_{th}(1) \cdot N_{S-1} \tag{10}$$

where N represents the number of pulses, $F_{th}(N)$ is the corresponding ablation threshold when the number of pulses is N, $F_{th}(1)$ is the ablation threshold corresponding to single pulse, and S is the coefficient of incubation effect. The laser source rewriting term in the two-temperature equation for simulating multi-pulsed laser has been described in Section 2.1.

Temperature analysis

Firstly, we would have a preliminary understanding of incubation effects by the temperature change of electron and lattice caused by the change of pulse number. The two-temperature curve of the material under the irradiation of single-pulsed, double-pulsed and multi-pulsed laser are as shown in Figs. 19 to 21, respectively. The laser fluence for each pulse is 1594 J/m², the pulse τ_L width is 300 fs, and the pulse interval dt_1 is 1 ps.

As can be seen from Fig. 20, after the first pulse, the electron rapidly heated up to 11718 K after 0.3 ps, transferred energy to the lattice, and the lattice continued to heat up. The second pulse was irradiated after 1 ps, the electron has cooled to 1380 K before the laser action, and the lattice was still warming. The injection of the second pulse energy caused the electron to reach a maximum temperature of 12403 K at 1.6 ps, after which the electron continued to transfer the energy to the lattice that was not fully heated. Then the electron and the lattice tended to be balance with the same trend after 3 ps. The lattice temperature caused by the first pulse is about 487 K, after the second pulse, the lattice temperature rose 556 K to reach the highest temperature. Compared to the single pulse action, the lattice has a more conspicuous temperature drop before the electron-phonon relaxation. Analyzing the two-temperature curve as Fig. 21 shown under the action of multi-pulsed laser, we find that both the electron and the lattice underwent three temperature rises, and the peak temperature of the three temperature rises is increasing. Since the pulse width and the pulse interval have not changed, the temperature change of the electron and the lattice under the first two pulses are consistent with the two-temperature curve under the action of the double pulse. After the third pulse, the electron reached the highest temperature of 12812 K at 2.9

ps, and the energy was transferred to the lattice. The lattice was heated to 1838 K at 3.5 ps. After 3.5 ps, the temperature of the electron and the lattice decreased and tended to be consistent.

It can be seen from the atomic snapshots in Figs. 22 to 24 that the increase of the number of pulses not only further increases the temperature of the electron and the lattice, but also actually reduces the ablation threshold of the material. The copper film in Fig. 22 only produces 'film respiration' under the irradiation of laser pulse with laser fluence of 1594 J/m^2. Increasing the number of pulses, we can see the nucleation inside of the material in Fig. 23, in the Fig. 24, we can find that there is a crack occurring and the ablation becomes more severe.

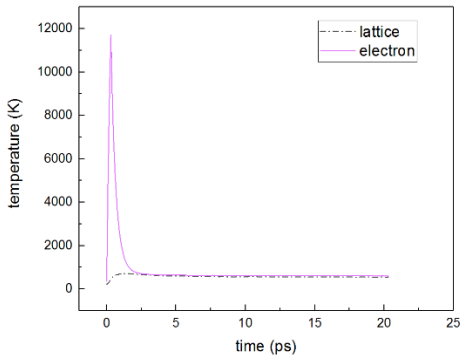

Fig. 19 Two-temperature curve under single-pulsed laser

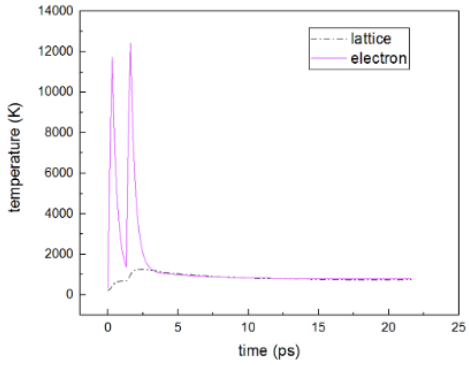

Fig. 20 Two-temperature curve under double-pulsed laser

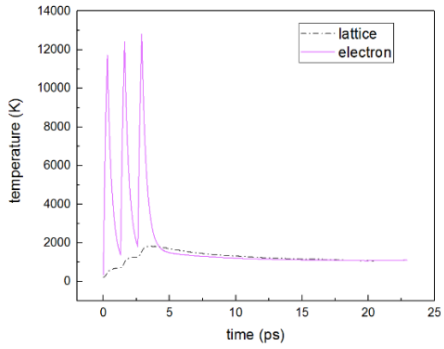

Fig. 21 Two-temperature curve under multi-pulsed laser

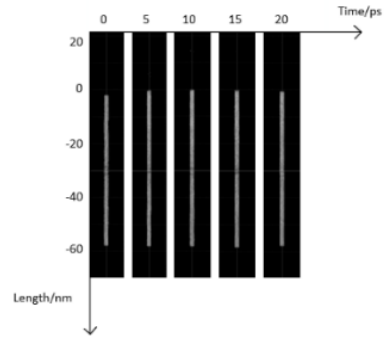

Fig. 22 Atomic snapshots under single-pulsed laser

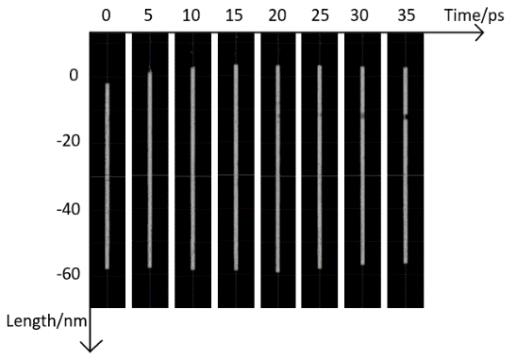

Fig. 23 Atomic snapshots under double-pulsed laser

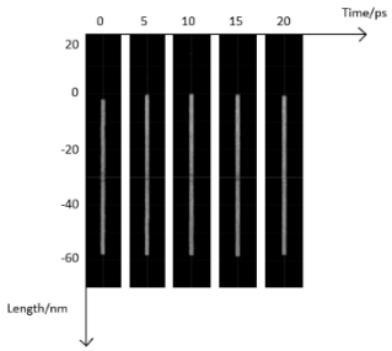

Fig. 24 Atomic snapshots under multi-pulsed laser

To further explore the temperature change of the electron and the lattice of each cross section of the material after the pulse action, we made a temperature contour with the time as the horizontal axis and the distance from the incident surface as the vertical axis as shown in Figs. 25 to 30.

Fig. 25 shows the electron temperature change of the internal sections of the metal material under the action of a single-pulsed laser. At 0.3 ps, the excitation made the electron 5 nm away from the incident surface rose to about 50000 K, the area with a large heat influence is 25 nm near the surface, which reached a maximum temperature of about 10000 K at 0.5 ps. Electron continuously transferred energy to the lattice through electron-phonon coupling. After 1 ps, the electron

temperature dropped below 5000 K. From Fig. 27, we can see that the electrons were excited twice, and the second laser was irradiated at 1.3 ps. At 1.6 ps, the electrons 5 nm from the front of the surface reached the highest temperature of about 55000 K, while the heat-affected zone was further expanded to 26.5 nm, and the electron temperature dropped back to 5000 K at around 2.2 ps. It can be seen from the temperature contour Fig. 29 that the highest temperature the electron could reach is 55000 K, which is the same as the highest temperature that can be achieved when the double-pulsed is applied. The difference is that the third pulse expands the heat-affected zone, and the electrons within 27 nm of the incident laser surface could be heated to more than 10000 K, and the thermal effect time of each pulse is also increased. As for the change of the lattice temperature, we can see from Fig. 26, Fig. 28 and Fig. 30 that the peak temperature of the lattice can be gradually increased due to the increase of the number of pulses, so as the heat-affected area.

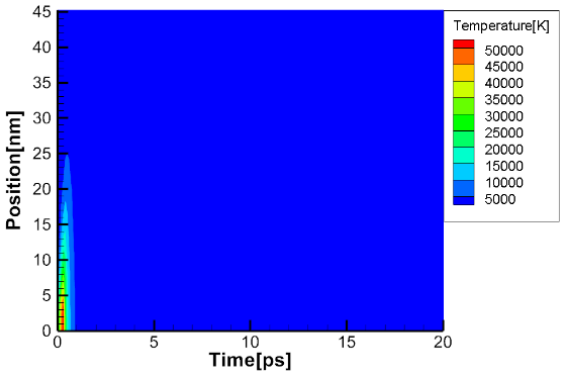

Fig. 25 Temperature contour of electron at laser fluence of 1594 J/m² under single-pulsed laser

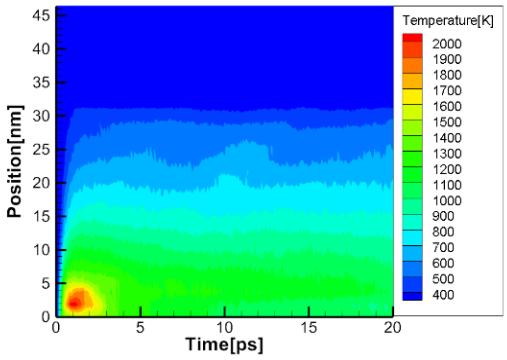

Fig. 26 Temperature contour of lattice at laser fluence of 1594 J/m² under single-pulsed laser

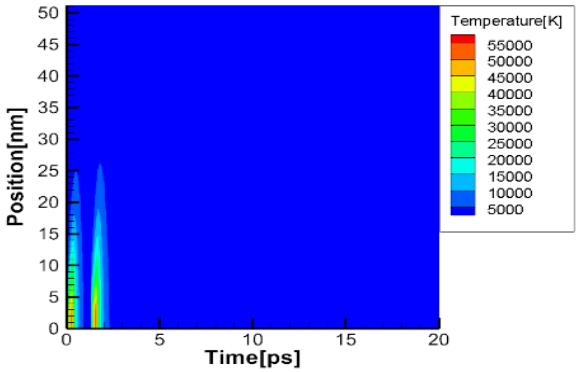

Fig. 27 Temperature contour of electron at laser fluence of 1594 J/m² under double-pulsed laser

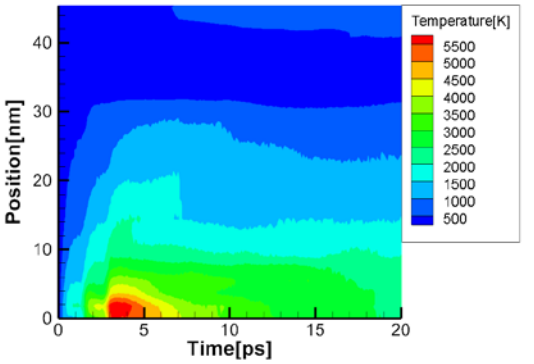

Fig. 28 Temperature contour of lattice at laser fluence of 1594 J/m² under double-pulsed laser

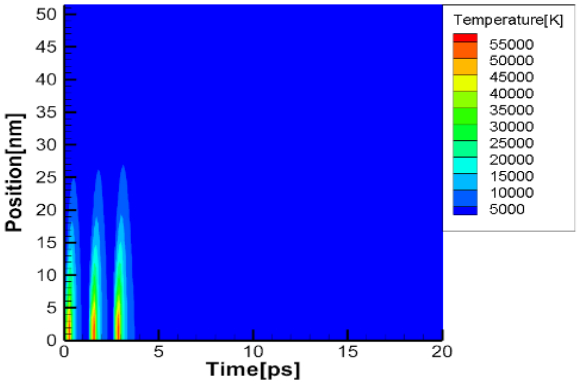

Fig. 29 Temperature contour of electron at laser fluence of 1594 J/m² under multi-pulsed laser

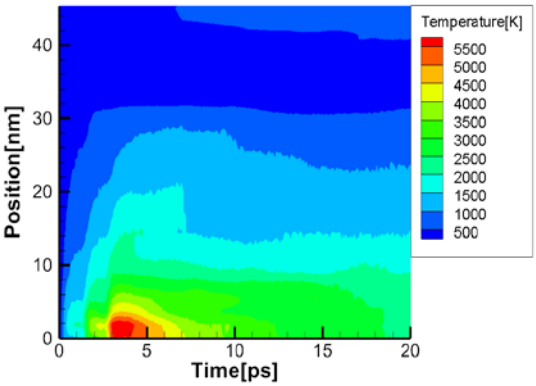

Fig. 30 Temperature contour of lattice at laser fluence of 1594 J/m² under multi-pulsed laser

Exploration of incubation effects

The existence of incubation effect causes the material to ablate at a single-pulse laser fluence that would otherwise not cause ablation, reducing the ablation threshold of the material. This is undoubtedly advantageous in engineering. However, in order to effectively remove the material, in addition to the research on the mechanism of action of multi-pulsed laser and metal, it is necessary to further explore the influencing factors of incubation effects. The greater the laser fluence, the more laser energy is injected into the system, and the ablation is more severe obviously.

In this section we would discuss the effect of pulse interval on the results of laser ablation of metals caused by multi-pulsed laser. Therefore, the fixed laser fluence and the pulse width $\tau_L$are 4782 J/m^2 and 300 fs, the pulse intervals of three groups we chose for the calculation are $dt_1 = 1$ ps, $dt_2 = 1$ ps; $dt_1 = 0.3$ ps, $dt_2 = 1$ ps and $dt_1 = 1$ ps, $dt_2 = 3$ ps, the calculated two-temperature curve are shown in Figs. 31 to 33.

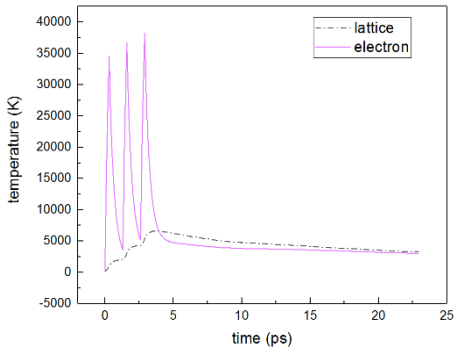

Fig. 31 Two-temperature curve when pulse interval are 1 ps, 1 ps

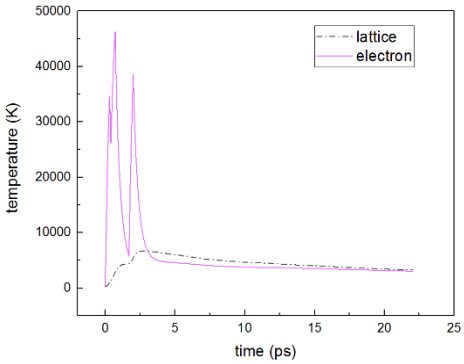

Fig. 32 Two-temperature curve when pulse interval are 0.3 ps, 1 ps

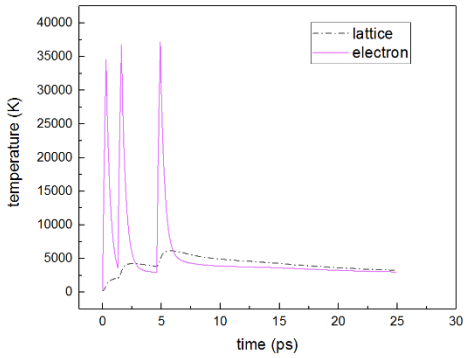

Fig. 33 Two-temperature curve when pulse interval are 1 ps, 3 ps

Analyzing the following three two-temperature curves Figs. 31 to 33, 1 ps is just about the approximate time required for the temperature to fall back after the electron rise to the peak temperature, which is roughly the time required for electron-phonon coupling, Therefore, when the pulse interval is 1 ps, the lattice temperature shows a steady upward trend. The highest lattice temperature appears at 3.7 ps, which is 6607 K, and the excited electron temperature can reach 21812 K.

When the first pulse interval is shortened to 0.3 ps, the electron temperature did not fall from the peak temperature completely when the second pulse irradiated. At the same time, the internal heat transfer of the electron and electron-phonon coupling was continuing, the thermal impact of the first pulse was still intense, the electron can be heated up to 46298 K, which is far greater than when the pulse interval of 1 ps. The energy obtained by the lattice is further increased, and the maximum temperature can reach 6697 K, which is also higher than the case when the pulse interval of 1 ps. Then we increase the second pulse interval to 3 ps, the temperature of the electron has dropped to 2955 K before the third pulse, and the peak temperature of the last pulse is only 37170 K, which is less than the above two cases.

According to the above analysis results, it can be found that the electron temperature, the lattice temperature, and the final equilibrium temperature are all improved when the pulse interval time is shortened to less than the electron-phonon coupling time. If the pulse interval time is longer than the electron-phonon coupling time, the inside of the material has already close to reaching the equilibrium state before the subsequent pulse action, and the effect of the energy of the subsequent pulse injection cannot be well exerted, which is not conducive to ablation. Therefore, the choice of pulse interval time is an important issue to improve the ablation efficiency. Shortening the pulse interval time is more conducive to energy accumulation.

Ablation depth is a visual representation of the pros and cons of processing results. In order to explore the influence of the important factor of the pulse interval on the ablation depth, the fixed pulse width is still 300 fs, and the first pulse interval is fixed at 1 ps. The second pulse interval for the four sets of calculations are 0.3 ps, 1 ps, 10 ps and 30 ps. To ensure the reliability of the calculation results, the visual result we obtain is shown in Fig. 34 by calculating 180,000 steps or 180 ps.

It can be seen from Fig. 34 that the ablation depth increases first and then decreases with the increase of the multi-pulsed laser time interval. Although the electron and the lattice can reach a higher temperature as shown in Fig. 31 at a pulse interval of 0.3 ps, the duration of the temperature above the ablation threshold is small compared to the case where the pulse time interval is close to the electron-phonon coupling time. Comparing the time when the first temperature rise of the electron reaches the peak to the start of the relaxation in Fig. 31 and Fig. 32, the pulse width is 3 ps at 0.3 ps, and the pulse width is about 5 ps at 1 ps. From this point of view, the pulse interval close to the electron-phonon coupling time allows the system to be maintained at a higher temperature for a longer time, resulting in an increase in the ablation depth. The shorter pulse interval makes the subsequent pulse and the pre-pulse to work together close to a single pulse, although a higher temperature is reached, but a shorter high temperature duration limits the increase in ablation depth. As the pulse interval is further increased to 10 ps and 30 ps, the thermal effect of the pre-pulse has been dissipated by the system, the lattice and electron temperatures have also fallen, and the ablation depth has gradually decreased. In summary, a pulse interval close to the electron-phonon coupling time of the material can complete a more efficient ablation of the material.

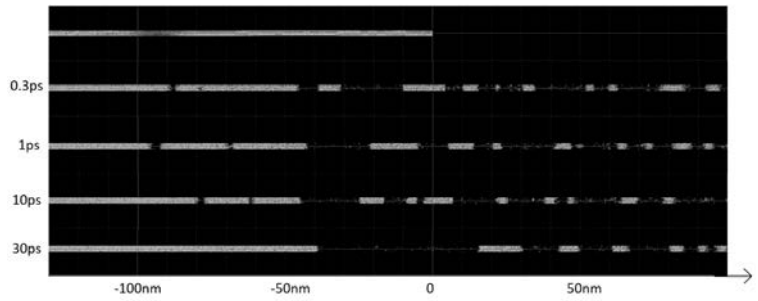

Fig. 34 Atomic snapshots of different pulse interval (at the moment of 180 ps)

4. Conclusion

The effect of ultrafast laser on metal is an extremely complex process with high imbalance, including the absorption of laser energy by electrons on the metal surface, the energy transfer from electron to the lattice through electron-phonon coupling and phonon collision, and the process of the lattice absorbs energy and causes the material to change phase. Finally, the surface of the material will be removed. To better describe the metal absorption process of laser ablates metallic materials, the researchers proposed a two-temperature model to describe the thermal conduction process of electrons and lattice systems of the material, while the two-temperature model is insufficient to explore the phase transition and ablation mechanism of metals during the unbalanced processes of laser processing. Therefore, molecular dynamics calculation is introduced to track the position and velocity of each atom by setting reasonable initial calculation conditions. We use

the EAM potential function and introduce periodic boundary conditions in the analysis of the interaction of metal and laser.

After establishing the appropriate size simulation system with the above method on the LAMMPS platform, we reproduced the ablation process of the single-pulsed laser to the metal and verified the correctness of our simulation. We firstly fixed the laser fluence and irradiated the surface of the copper film with lasers of different pulse widths. It was found that when the pulse width is reduced, the pulse energy is more concentrated, and the lattice and electrons inside the system can reach a higher peak temperature. Moreover, the smaller the pulse width, the faster the electron temperature rises. Then, the pulse width was set to a fixed value, the metal was irradiated with laser of different laser fluences, and the visualized atomic snapshots was analyzed. In the visualization results, the nucleation of voids when the laser fluence is small and the nucleation of bubbles inside the material when the laser fluence is large were observed. The larger laser fluence causes the layer cracking of the material, so that more materials are removed. After understanding the ablation mechanism, the calculation system was enlarged to eliminate the effect of thermal expansion. The laser ablation depth at different energy densities was calculated, the fitting curve was obtained, and compared with the literature.

Multi-pulsed laser ablation is not a simple superposition of single-pulsed laser. The process of interaction with metal is more complicated. In this paper, the multi-pulsed laser ablation was calculated by changing the light source term in the two-temperature equation. Comparing the temperature contour and atomic snapshots of multi-pulsed laser action and single-pulsed laser action, we found that the increase of the number of laser pulses reduces the ablation threshold of the material. The nucleation and phase change inside the material is more severe due to the increase of energy, the lattice disorder is more serious, and the ablation becomes faster. Then we discussed the influence of pulse interval time on the incubation effect of multi-pulsed laser. The pulse interval time is shorter than the electron-phonon coupling time, which makes the temperature of the system more intense. If the pulse interval is too long, the energy will be dissipated at the pulse interval. Therefore, the appropriate pulse interval should be selected during the laser processing.

It should be noted that although copper was chosen as the target material in this study due to the abundant research of its thermophysical properties, the method of molecular dynamic modeling and analysis can be applied to other metallic material as long as the detailed thermophysical parameters of the materials determined. The results obtained in this work can provide a new calculation method and theoretical basis for ultra-fast laser machining of air film holes in aviation turbine blades and has certain practical guiding significance for laser machining.

Acknowledgements

The material presented in this paper is based upon work supported by the National Natural, Science Foundation of China (Grant Number 51705440), the Fundamental Research Funds for the Central Universities XMU (Grant Number 20720180072), the Aeronautical Science Foundation of China (Grant Number 20170368001), the Shenzhen Fundamental Research Program (Grant Number JCYJ20170818141303656), and the Natural Science Foundation of Fujian Province, China (Grant Number 2019J01044), National Science and Technology Major Project (J2019-III-0008), National Science and Technology Major Project (J2019-VII-0013-0153), Research Project (PZ2020016).

References

[1] Mills, B., Heath, D.J., Grant-Jacob, J.A., Eason, R.W. (2018). Predictive capabilities for laser machining via a neural network, *Optics Express*, Vol. 26, No. 13, 17245-17253, doi: 10.1364/OE.26.017245.

[2] Rethfeld, B., Ivanov, D.S., Garcia, M.E., Anisimov, S.I. (2017). Modelling ultrafast laser ablation, *Journal of Physics D: Applied Physics*, Vol. 50, No. 19, Article No. 193001, doi: 10.1088/1361-6463/50/19/193001.

[3] Templeton, J.A., Jones, R.E., Wagner, G.J. (2010). Application of a field-based method to spatially varying thermal transport problems in molecular dynamics, *Modelling and Simulation in Materials Science and Engineering*, Vol. 18, No. 8, Article No. 085007, doi: 10.1088/0965-0393/18/8/085007.

[4] Bogaerts, A., Aghaei, M., Autrique, D., Lindner, H., Chen, Z.Y., Wendelen, W. (2011). Computer simulations of laser ablation, plume expansion and plasma formation, *Advanced Materials Research,* Vol 227, 1-10, doi: 10.4028/www.scientific.net/AMR.227.1.

[5] Ivanov, D.S., Zhigilei, L.V. (2003). Combined atomistic-continuum modeling of short-pulse laser melting and disintegration of metal films, *Physical Review B*, Vol. 68, No. 6, Article No. 064114, doi: 10.1103/PhysRevB.68.064114.

[6] Amouye Foumani, A., Niknam, A.R. (2018). Atomistic simulation of femtosecond laser pulse interactions with a copper film: Effect of dependency of penetration depth and reflectivity on electron temperature, *Journal of Applied Physics*, Vol. 123, No. 4, 043106, doi: 10.1063/1.5009501.
[7] Povarnitsyn, M.E., Fokin, V.B., Levashov, P.R. (2015). Microscopic and macroscopic modeling of femtosecond laser ablation of metals, *Applied Surface Science*, Vol. 357, Part A, 1150-1156, doi: 10.1016/j.apsusc.2015.09.131.
[8] Liang, J.-G., Ni, X.-C., Yang, L., Wang, Q.-Y. (2005). Numerical simulation of the ablation on copper with ultrashort laser pulses, *China Laser*, Vol. 32, No. 9, 1291-1294, doi: 10.3321/j.issn:0258-7025.2005.09.029.
[9] Winter, J., Rapp, S., Schmidt, M., Huber, H.P. (2017). Ultrafast laser processing of copper: A comparative study of experimental and simulated transient optical properties, *Applied Surface Science*, Vol. 417, 2-15, doi: 10.1016/j.apsusc.2017.02.070.
[10] Wang, Q., Luo, S., Chen, Z., Qi, H., Deng, J., Hu, Z. (2016). Drilling of aluminum and copper films with femtosecond double-pulse laser, *Optics & Laser Technology*, Vol. 80, 116-124, doi: 10.1016/j.optlastec.2016.01.001.
[11] Karim, E.T., Shugaev, M.V., Wu, C., Lin, Z., Matsumoto, H., Conneran, M., Kleinert, J., Hainsey, R.F., Zhigilei, L.V. (2016). Experimental characterization and atomistic modeling of interfacial void formation and detachment in short pulse laser processing of metal surfaces covered by solid transparent overlayers, *Applied Physics A*, Vol. 122, Article No. 407, doi: 10.1007/s00339-016-9944-7.
[12] Fokin, V.B., Povarnitsyn, M.E., Levashov, P.R. (2017). Simulation of ablation and plume dynamics under femtosecond double-pulse laser irradiation of aluminum: Comparison of atomistic and continual approaches, *Applied Surface Science*, Vol. 396, 1802-1807, doi: 10.1016/j.apsusc.2016.11.208.
[13] Wu, Z., Dong, Y., Zhang, S., Liao, T., Yan, W., You, Y. (2021). Discussion on effect of laser parameters and trajectory in combined pulse laser drilling, *International Journal of Hydromechatronics*, Vol. 4, No. 1, 43-54, doi: 10.1504/IJHM.2021.114175.
[14] Anisimov, S.I., Kapeliovich, B.L., Perelman, T.L. (1974). Electron emission from metal surfaces exposed to ultrashort laser pulses, *Soviet Journal of Experimental and Theoretical Physics*, Vol. 66, No. 2, 375-377.
[15] Zhang, Z., Xu, Z., Wang, C., Liu, S., Yang, Z., Zhang, Q., Xu, W. (2021). Molecular dynamics-guided quality improvement in the femtosecond laser percussion drilling of microholes using a two-stage pulse energy process, *Optics & Laser Technology*, Vol. 139, Article No. 106968, doi: 10.1016/j.optlastec.2021.106968.
[16] Qui-lin, X., Li, Z., Xiao-geng, T. (2015). Ultrafast thermomechanical responses of a copper film under femtosecond laser trains: A molecular dynamics study, *Proceedings of the Royal Society A: Mathematical, Physical and Engineering Sciences*, Vol. 471, Article No. 20150614, doi: 10.1098/rspa.2015.0614.
[17] Rethfeld, B., Ivanov, D.S., Garcia, M.E., Anisimov, S.I. (2017). Modelling ultrafast laser ablation, *Journal of Physics D: Applied Physics*, Vol. 50, No. 19, Article No. 193001, doi: 10.1088/1361-6463/50/19/193001.
[18] Momma, C., Nolte, S., Chichkov, B.N., Alvensleben, F.v., Tünnermann, A. (1997). Precise laser ablation with ultrashort pulses, *Applied Surface Science*, Vol. 109-110, 15-19, doi: 10.1016/S0169-4332(96)00613-7.
[19] Zhang**,** Y.-F., Wang**,** L.-L., Gong**,** J.-L. (2016). Numerical simulation of femtosecond laser multi-pulse ablation of Ni-Ti alloy, *Journal of Photonics*, Vol. 45, No. 5, Article No. 0514002, doi: 10.3788/gzxb20164505.0514002.
[20] Lasemi, N., Pacher, U., Zhigilei, L.V., Bomati-Miguel, O., Lahoz, R., Kautek, W. (2018). Pulsed laser ablation and incubation of nickel, iron and tungsten in liquids and air, *Applied Surface Science*, Vol. 433, 772-779, doi: 10.1016/j.apsusc.2017.10.082.